IEEE Access
Multidisciplinary ⋮ Rapid Review ⋮ Open Access Journal

Received September 27, 2019, accepted October 9, 2019, date of publication October 22, 2019, date of current version November 22, 2019.

Digital Object Identifier 10.1109/ACCESS.2019.2947621

Misfire Detection Based on Generalized Force Identification at the Engine Centre of Gravity

CHUANYAN XU, SHAN LI, FENGPING CAO, AND XUYUN QIU
School of Automotive Engineering, Shandong Jiaotong University, Jinan 250023, China

Corresponding author: Chuanyan Xu (xcy@sdjtu.edu.cn)

This work was supported by the National Natural Science Foundation of China (Grant No. 51405272, 51505258) and was also partly supported by the Key Research and Development Program of Shandong (2016GNC112010, 2017NC212002) and the Agricultural Machinery Equipment Research and Development Innovation Program Project of Shandong (2017YF013, 2018YF017) funding and Open Subject of Traffic Safety and Control Lab in Hebei Province (Grant No. JTKY2019002).

ABSTRACT Misfiring creates a unique pattern attributed to a particular cylinder. When a misfire occurs, the balance of the engine is destroyed, and the generalized force at the centre of gravity (C.G.) of the engine is changed. In this paper, a new misfire detection method is presented based on the identification of the generalized force at the engine centre of gravity. Based on the engine acceleration signals at the mounts, through the use of the discrete spectrum interpolation method, the accurate amplitudes and phases of the acceleration signals are extracted, and then, the generalized force at the centre of gravity is calculated. Through analysing the main harmonic orders of the generalized force, the misfire features are accurately extracted and classified. Both the simulation examples and test bed results prove the effectiveness of the present method in detecting misfire faults in combustion engines.

INDEX TERMS Engine, misfire detection, the centre of gravity, the generalized force.

I. INTRODUCTION

Structural dynamical monitoring and fault diagnosis are of great importance to structural health. Many works have been presented addressing structural health monitoring and equipment evaluation [1]–[4]. An engine misfire fault is a common combustion fault in internal combustion (IC) engines and leads to severe performance degradation and a large increase of hydrocarbon emissions. Overall, engine misfire diagnosis is traditionally based on the in-cylinder factor and post-cylinder factor. In-cylinder factor diagnosis methods mainly use the ion current signal [5], [6], optical signal [7] and cylinder pressure signal [8] to detect engine misfires. Post-cylinder factor methods apply features such as the instantaneous crankshaft angular velocity [9], instantaneous angular acceleration [10], crankshaft combustion torque [11], crank angle [12], engine vibration signal [13], exhaust gas pressure [14], exhaust gas temperature [15] and engine noise [16], [17] to detect misfire faults. The measurement of the in-cylinder factor requires mounting a special sensor inside the engine, and by contrast, the measurement of the post-cylinder factor requires little change to the engine and is favoured by researchers. Benefiting from complete test equipment, reliable diagnosis results and convenient real-time diagnosis, vibration-based methods for engine misfire detection have been intensively studied [18]–[20]. For example, Arroyo *et al.* [12] proposed a diagnosis method achieved by comparing the vibration and AE energy with reference values to determine whether an engine is in a faulty condition. Devasenapati *et al.* [21] used the vibration signal acquired from the engine by a piezoelectric accelerometer to identify misfires in a four-stroke four-cylinder petrol engine. In this work, a decision tree was used to select and classify the features. Since misfiring creates a unique vibration pattern attributed to a particular cylinder, Sharma *et al.* [22] extracted the statistical features of engine block vibration signals and detected misfire faults using a series of decision trees. However, the diagnosis accuracy of vibration-based misfire detection methods is affected by many factors such as complex engine construction, heavy noise, the temperature and the sensor installation position. The inherent vibration forces induced in engines are mainly due to the reciprocating inertial force, rotational inertia force and gas explosive force. The vibrational pattern of an engine can provide a variety of engine state information. The direct expression of most engine faults is the variation of the generalized force at the centre of gravity of the engine. For example, for an inline four-cylinder four-stroke engine, during normal engine

The associate editor coordinating the review of this manuscript and approving it for publication was Dong Wang.

operation, the inertia force among the cylinders can be cancelled, and the horizontal force at the centre of gravity is nearly zero. The main vertical force is the second-order force, while the first-order force is close to zero [23]. However, when a misfire occurs, the equilibrium relations among the cylinders are destroyed, and the force at the centre of gravity is also changed. The method of misfire detection presented in this paper is based on the estimation of the generalized force at the gravity centre of the engine. The proposed method features two benefits—one is high fault sensitivity, and the other is that the method is less affected by the external environment and test conditions.

The rest of the paper is organized as follows. The generalized force estimation method is introduced in Section II. Misfire detection is presented in Section III. The measurement results are given in Section V. Finally, the conclusions are drawn in Section VI.

II. THE GENERALIZED FORCE ESTIMATION

The generalized force at the gravity centre of an engine is normally calculated based on the engine parameters [24], which are the gas explosion force, reciprocating inertial force, and rotating inertia force. The engine-mount system can be simplified as a six-degrees-of-freedom vibration model, and under the assumption of "small" motions, the engine-mount system equations can be expressed as

$$\mathbf{M}\ddot{\mathbf{Q}}(t)+\mathbf{C}\dot{\mathbf{Q}}(t)+\mathbf{K}\mathbf{Q}(t)=\mathbf{F}(t) \tag{1}$$

After conducting a Fourier transformation on both sides, then equation (1) becomes

$$\left[\mathbf{M}-\frac{\mathbf{K}}{(2\pi f)^2}-\frac{j\mathbf{C}}{2\pi f}\right]\ddot{\mathbf{Q}}(f)=\mathbf{F}(f) \tag{2}$$

where $\mathbf{M}$ is the 6×6 engine's rigid mass matrix, $\mathbf{C}$ is the 6×6 damping matrix, $\mathbf{K}$ is the 6×6 stiffness matrix, $\mathbf{Q}$ is the generalized displacement vector at the C.G. of the engine and $\mathbf{F}$ is the 6×1 generalized force vector.

Consider that s acceleration measurement points are applied. The coordinates of $kth(k=1,\cdots,s)$ point relative to the C.G. are $[x_k\ y_k\ z_k]$, and under the assumption of "small" motions, we can get

$$\mathbf{A}=\mathbf{E}\ddot{\mathbf{Q}} \tag{3}$$

where $\mathbf{E}$ is the transpose matrix and $\mathbf{A}$ is the acceleration vector of all points with three orthogonal directions.

$$\mathbf{E}=\begin{bmatrix} 1 & 0 & 0 & 0 & z_1 & -y_1 \\ 0 & 1 & 0 & -z_1 & 0 & x_1 \\ 0 & 0 & 1 & y_1 & -x_1 & 0 \\ & & & \cdots & & \\ 1 & 0 & 0 & 0 & z_s & -y_s \\ 0 & 1 & 0 & -z_s & 0 & x_s \\ 0 & 0 & 1 & y_s & -x_s & 0 \end{bmatrix}$$

Then, $\ddot{\mathbf{Q}}$ can be determined in a least-squares sense as

$$\ddot{\mathbf{Q}}=\left(\mathbf{E}^{\mathrm{T}}\mathbf{E}\right)^{-1}\mathbf{E}^{\mathrm{T}}\mathbf{A} \tag{4}$$

According to the acceleration signals at the engine mounts, through the interpolation method of the discrete spectrum, the accurate amplitudes and phases of the acceleration signals can be extracted. According to equations (2) and (4), the generalized force at the centre of gravity can be calculated by the following equation [25].

$$\mathbf{F}(f)=\left[\mathbf{M}-\frac{1}{\omega^2}\mathbf{K}^*\right]\left(\mathbf{E}^{\mathrm{T}}\mathbf{E}\right)^{-1}\mathbf{E}^{\mathrm{T}}\mathbf{A} \tag{5}$$

Compared to the gas-pressure torque, the reciprocating inertia torque imposes a minimal influence on the crankshaft's vibration since it only affects the size of the vibration and does not generate any useful external power. For an engine with i cylinders, every cylinder's gas-pressure torque has a phase difference of $4\pi/i$, which varies according to the firing order of the engine. Fig. 1 illustrates the phase angle diagram for the gas pressure torque of a typical four-stroke four-cylinder engine with the firing order of 1-3-4-2. According to Fig. 1, if all cylinders contribute equally to the engine torque, only the main harmonic orders, which are multiples of half of the number of cylinders in a four-stroke engine, will survive in the harmonic structure of the resultant torque due to gas forces. This means that the first main harmonic order k = i/2 has the largest amplitude on the spectrum of the resultant torque. Thus, for the four-stroke four-cylinder engine, the main harmonic orders are k = i/2, i, 3i/2, etc**.** According to equation (1), the main harmonic orders of the resultant torque are the 2nd, 4th and 6th orders under normal operation. When a misfire occurs, the main harmonic orders will be changed.

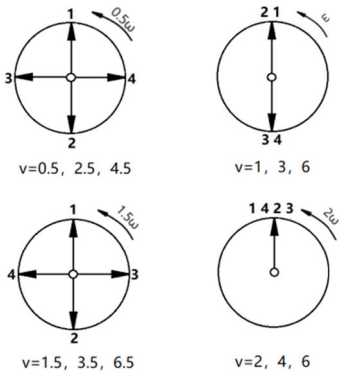

FIGURE 1. Phase angle diagrams for the gas pressure torque of a typical four-stroke four-cylinder engine.

III. MISFIRE DETECTION BASED ON THE IDENTIFICATION OF THE GENERALIZED FORCE

In this section, a high-quality finite element and multi-body dynamics model of a four-cylinder inline engine with mounts is designed based on AVL-Excite. Due to the high degrees of freedom of the finite element model, the matrix is reduced by MSC Nastran to reduce the size of the solution. The reduced finite element model is imported into the EXCITE Power Unit. The logical diagram of the component connections is

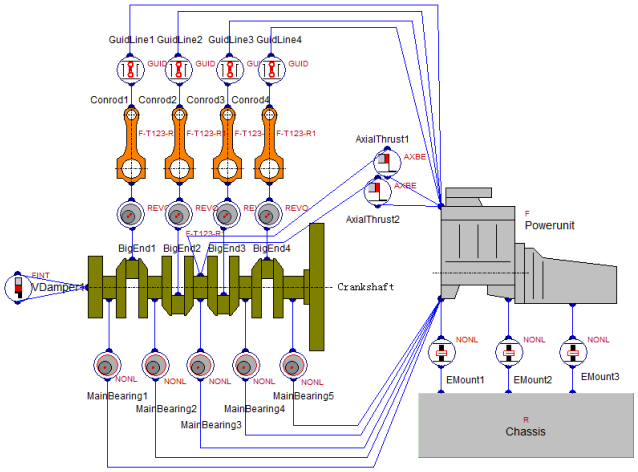

FIGURE 2. Logical diagram of the component connections.

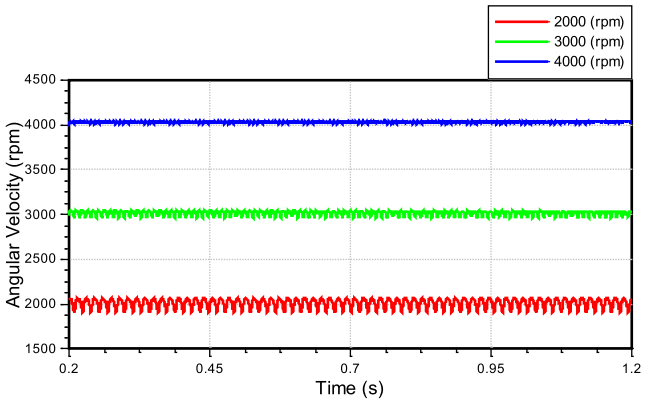

FIGURE 3. Crankshaft speed fluctuation.

shown in Fig. 2. The angular velocity of the crankshaft is extracted to observe the rotational speed fluctuation of the engine model to confirm that there is no abnormal crankshaft movement or stagnation during the engine operation. The explosion pressure of each cylinder is provided by the cylinder pressure curve. The crankshaft speed fluctuations simulated at 2000rpm, 3000rpm, and 4000rpm are shown in Fig. 3. The figure shows that the crankshaft runs smoothly, the simulation model runs well under the operation conditions and the computation results are reliable. The acceleration signal at 2000rpm with the rotational frequency of 33.3 Hz is shown in Fig. 4. For the inline 4-cylinder engine vibration, the second, fourth and sixth harmonics are the main harmonic orders. From Fig. 4, we can see that the second harmonic, i.e., 66.67Hz, has the largest amplitude on the spectrum, followed by those of the other harmonic orders, and the simulation results are in accordance with the actual engine performance.

The c.g. of the powertrain and the position of the mounts are listed in Table 1. The inertia parameters of the powertrain except for the crankshaft, connecting rod and piston are listed in Table 2, and the static stiffness of the three mounts is

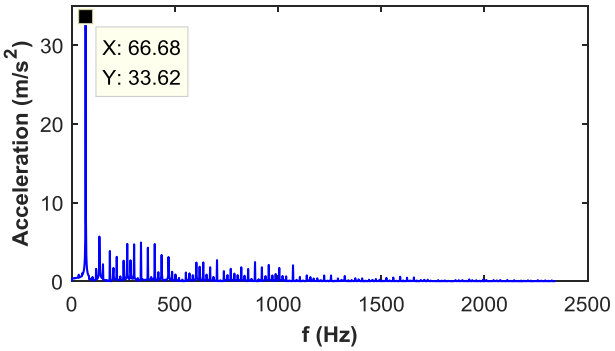

FIGURE 4. Vibration signal at 2000 rpm.

3×10^5N/m, while the damping is 200 N · s/m. In the present study, we use the model to simulate four different cases, i.e., normal, single misfire, intermittent double-cylinder misfire, and continuous double-cylinder misfire conditions. The running speed of the engine is 2000 rpm.

TABLE 1. C.G. of the engine and the positions of the mounts.

	X	*Y*	*Z*
Engine c.g.	139.3 mm	9.8 mm	91.9 mm
Mount 1	0	285.2 mm	122 mm
Mount 2	73 mm	-254 mm	-45.5 mm
Mount 3	554.5 mm	-80.4 mm	-148.1 mm

A. NORMAL

The firing order of the engine is 1-3-4-2. Under normal conditions, according to the phase angle diagrams, the main harmonic orders of the vibration signal of the engine are the 2nd, 4th, and 6th orders. That is, the second harmonic has the largest amplitude on the spectrum of the resultant torque, and the vibration signal of the engine block also follows the same basic law. The acceleration signals at the three mounts are used to calculate the generalized force at the centre of gravity of the engine. The interpolation method using a Hanning window is applied for the extraction of the frequency, amplitude and phase, and the generalized force at the centre of gravity can be accurately identified according to equation (1). The calculation method below is similar. Since the vertical load is dominant for the inline 4-cylinder engine, in this paper, only the vertical generalized force is analysed for feature extraction. The identified vertical generalized force at the centre of the gravity is shown in Fig. 5. We can see that the 2nd harmonic has the largest amplitude and that the 4th harmonic has the second largest amplitude.

B. SINGLE MISFIRE

The misfire fault is simulated by setting the cylinder pressure value to one at which an explosion does not occur. Based on

TABLE 2. Inertia parameters of the engine.

Mass	Moment of inertia			Product of inertia		
m	J_{xx}	J_{yy}	J_{zz}	J_{xy}	J_{yz}	J_{xz}
111 kg	4.13 kg· m^2	9.67 kg· m^2	8.13 kg· m^2	0.16 kg· m^2	-0.16 kg· m^2	1.12 kg· m^2

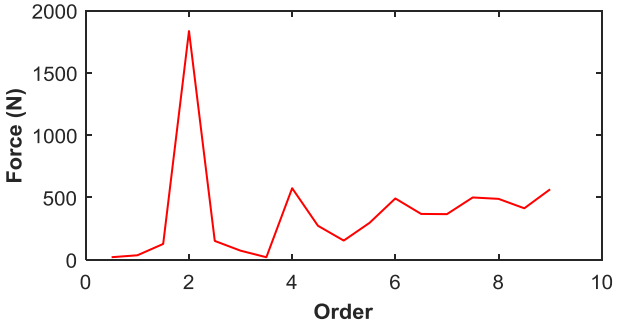

FIGURE 5. Identified vertical generalized force at the C.G. of the engine.

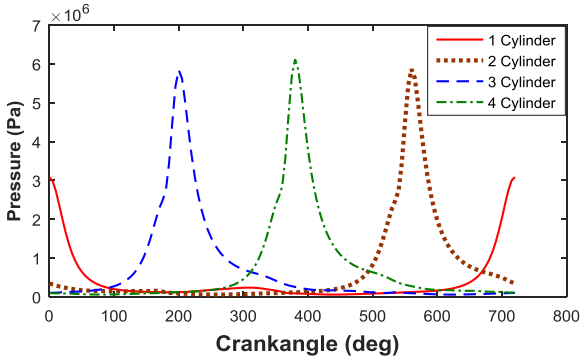

FIGURE 6. Pressure curve with a misfire of the first cylinder at 2000 rpm.

AVL Boost and the above engine model, a thermodynamic model at 2000 rpm is designed to generate misfire pressure curve, and the air-fuel ratio is set to infinity to simulate a misfire. The pressure curves of the engine with misfiring of the first cylinder are shown in Fig. 6.

The identified generalized force is shown in Fig. 7. We can see that the 2nd harmonic has the largest amplitude, which is similar to the case without a misfire shown in Fig.5. However, the amplitudes of 0.5th, 1st and 1.5th harmonics increase sharply in Fig. 7. Once a single misfire occurs, the balance of the engine is destroyed, the gas explosion forces of other three firing cylinders form a new cycle, the rate of change is half of the engine speed, and the corresponding 0.5th harmonic and its multiples appear.

C. INTERMITTENT DOUBLE-CYLINDER MISFIRE

A misfire is set in cylinders 1 & 4 to simulate the intermittent double-cylinder misfire fault.

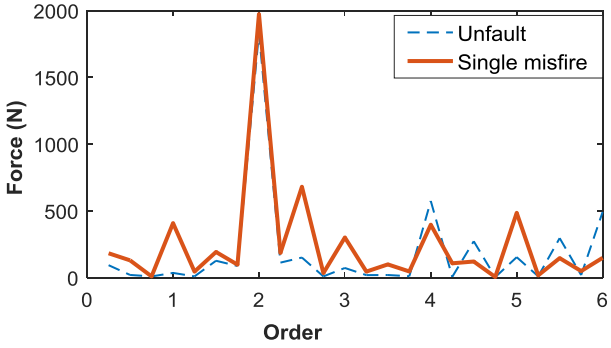

FIGURE 7. Vertical generalized force of a single misfire.

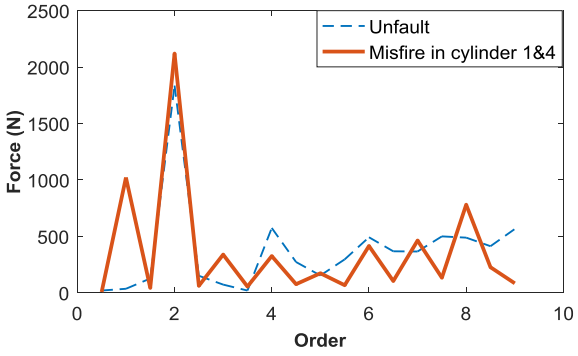

FIGURE 8. Vertical generalized force of an intermittent double-cylinder misfire.

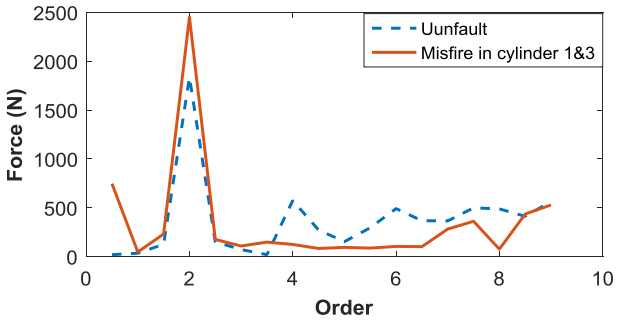

FIGURE 9. Generalized force of a continuous double-cylinder misfire.

From Fig. 8, we can see that due to the intermittent misfires, the frequency of the gas explosion forces becomes one-half of that under normal conditions, and the generalized force appears in the 1st harmonic, along with its multiples.

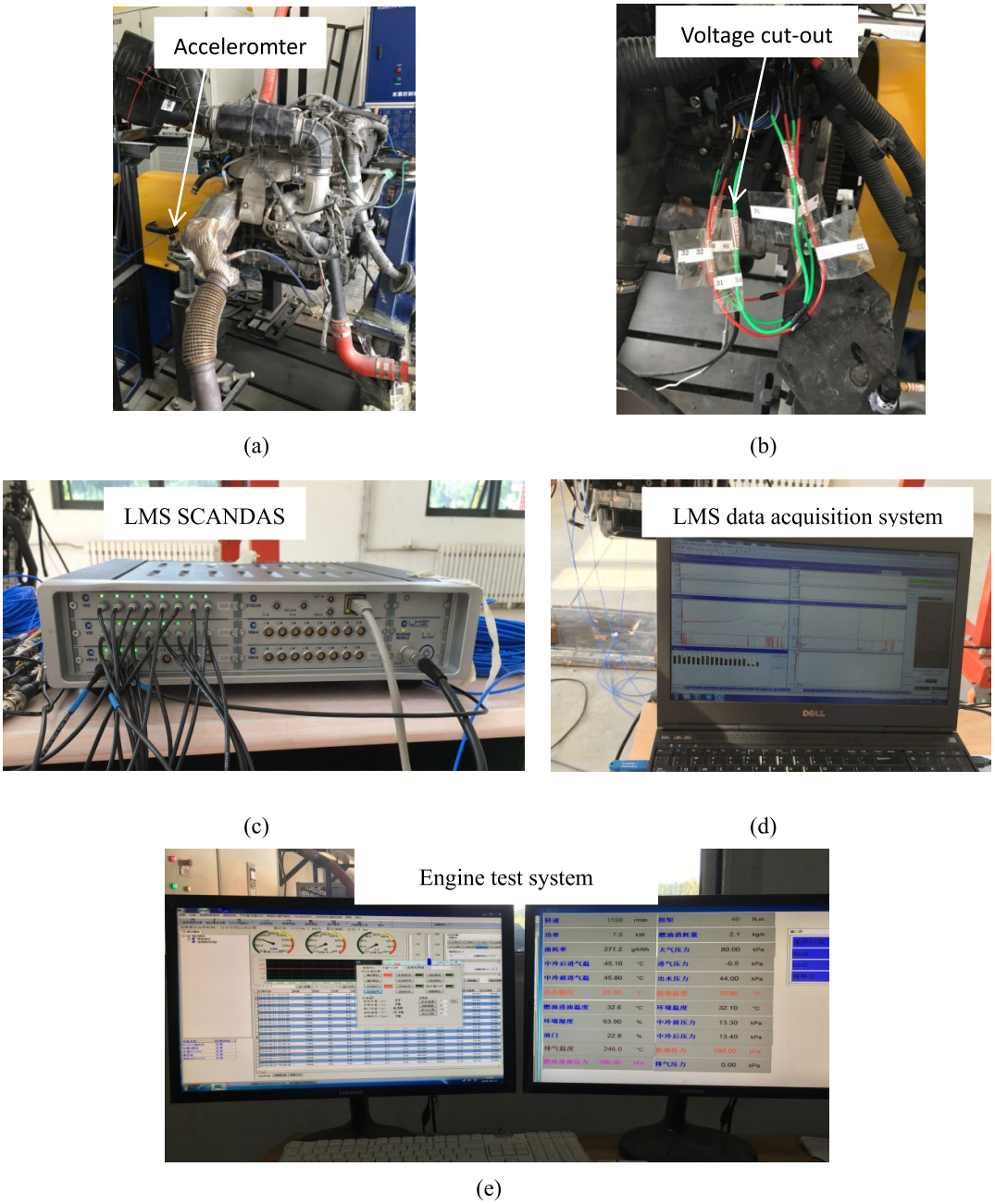

FIGURE 10. Engine setup: (a) experimental engine, (b) voltage-controlled switch, (c) signal conditioner, (d) data acquisition system, (e) test rig console.

D. CONTINUOUS DOUBLE–CYLINDER MISFIRE

A misfire is set in cylinders 1 & 3 to simulate the continuous double-cylinder misfire fault. In this case, a misfire leads to the excitation force forming another cycle, that is, the crankshaft turns twice during one cycle; thus, the amplitude the 0.5^{th} harmonic increases sharply, as shown in Fig. 9.

IV. EXPERIMENTAL SETUP

The misfire simulation consists of two subsystems: an IC engine test rig and a data acquisition system.

A. IC ENGINE SYSTEM

The experimental setup of the engine misfire simulator consists of a four-stroke inline four-cylinder gasoline engine (160.5 Kg). The engine is attached to the test bed by three rubber mounts and is operated by the engine control system. A misfire fault is simulated by switching off the high-voltage electrical supply to individual spark plugs.

B. DATA ACQUISITION SYSTEM

Three triaxial acceleration sensors are used to measure the vibration above the mounts, and three uniaxial acceleration

TABLE 3. Inertia parameters of the engine.

Mass	Moment of inertia			Product of inertia		
m	J_{xx}	J_{yy}	J_{zz}	J_{xy}	J_{yz}	J_{xz}
162.8 kg	7.63 kg· m^2	16.83 kg· m^2	13.4 kg· m^2	-1.02 kg· m^2	-0.39 kg· m^2	4.40 kg· m^2

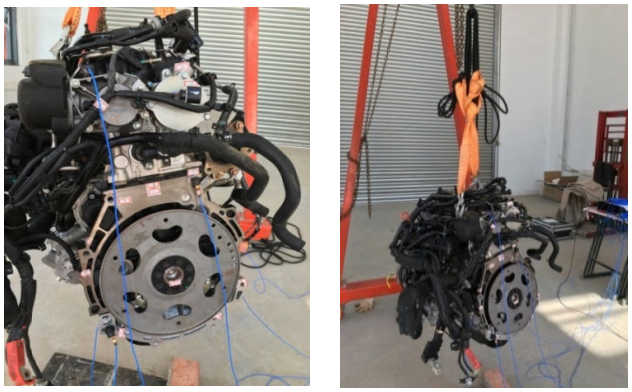

FIGURE 11. Test engine in the free-free condition.

sensors are used to measure the vibration under the mounts. The acceleration signals are measured and processed by a multi-channel LMS SCANDAS analyser, allowing for the simultaneous acquisition of 40 responses and one force in a conventional test. The engine test rig and data acquisition system are shown in Fig. 10.

C. INERTIA PARAMETERS AND THE RUBBER ELEMENTS

According to equation (1), the parameters of the engine components should be measured or calculated first. The engine inertia parameters are identified by a residual inertia method that allows the simultaneous estimation of all ten parameters. The engine is suspended from very soft springs to simulate free-free boundary conditions, as shown in Fig. 11. Five response measurement points and 26 applied forces were considered. The coordinates of the measuring points were measured by a 3D coordinate measuring apparatus. The FRFs were measured with the sampling frequency of 512 Hz and1024 sampling points. The modulus values of the FRFs calculated for the response measurement points are presented in Fig. 12. As shown in Fig. 12(a), the first elastic resonance frequency is approximately 202 Hz, with a low amplitude value. From Fig. 12(b), we can see that the mass line between 70 Hz and 144 Hz is smooth enough for the accurate estimation of the inertia parameters. The details of the calculation of the inertia parameters can be found in our previous work [26]. The calculated results are shown in Table 3.

Fig. 13 illustrates the static and dynamic testing of the rubber elements by the MTS. Since vertical vibration is

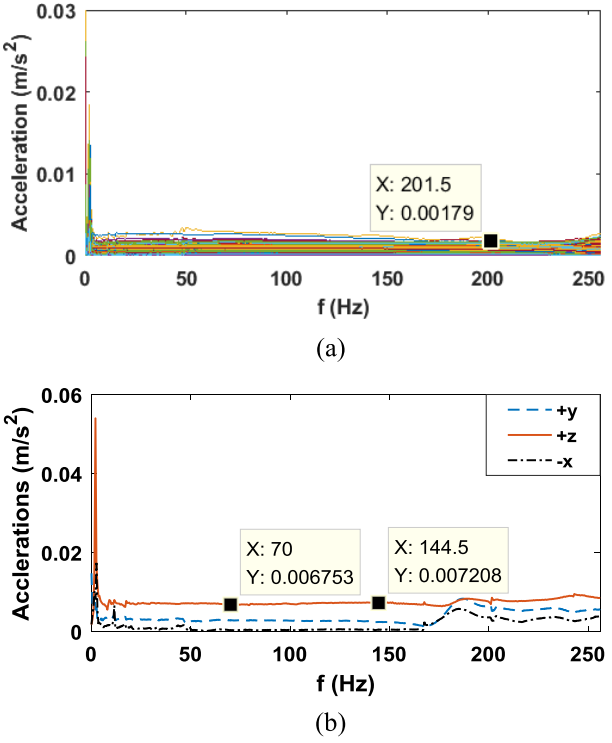

FIGURE 12. Amplitude-frequency response for the measurement points: (a) FRFs for all points, (b) an example of measured FRFs.

dominant for the inline 4-cylinder engine, only the vertical dynamic stiffness was tested. During testing, a 550 N pre-load was applied, according to the actual load on a single rubber element, and harmonic displacement excitations with a frequency of 0.01 Hz at 0.15 mm were employed. The ambient temperature was maintained at 23 ± 2 °C. The test results of the static and dynamic stiffness are shown in Figs. 14-16, respectively.

D. SIMULATION OF MISFIRE

As mentioned above, the engine is running under four cases, i.e., normal, single misfire, intermittent double-cylinder misfire, and continuous double-cylinder misfire conditions. The engine is started by an electrical control system and warmed up for 10 min before testing. The accelerometers are initialized and the data are recorded after the engine speed stabilized. The sampling frequency and the sampling points

(a) (b)

(c)

FIGURE 13. Static and dynamic testing of the rubber element: (a) vertical static stiffness test, (b) lateral static stiffness test, (c) dynamic stiffness test.

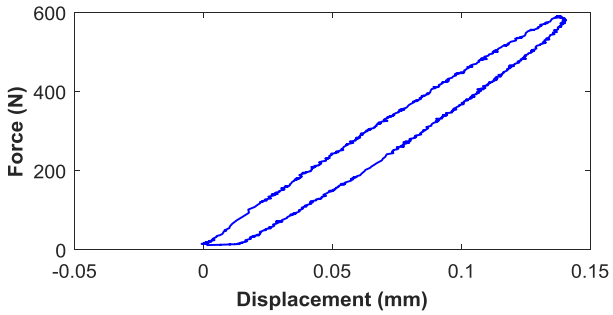

FIGURE 14. Hysteresis loops for the vertical static test.

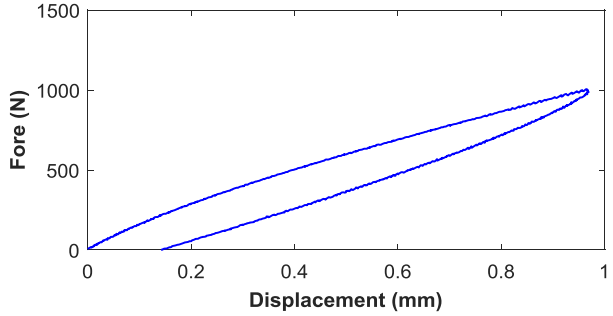

FIGURE 15. Hysteresis loops for the lateral static test.

are set as 4096 Hz and 8192, respectively. Additionally, the interpolation method for the discrete spectrum with a Hanning window is used to extract the frequency, amplitude

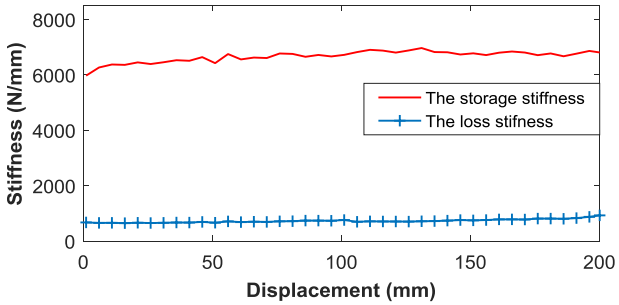

FIGURE 16. Tested dynamic stiffness.

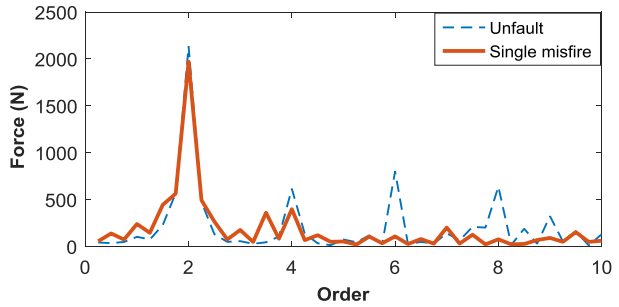

FIGURE 17. Single misfire.

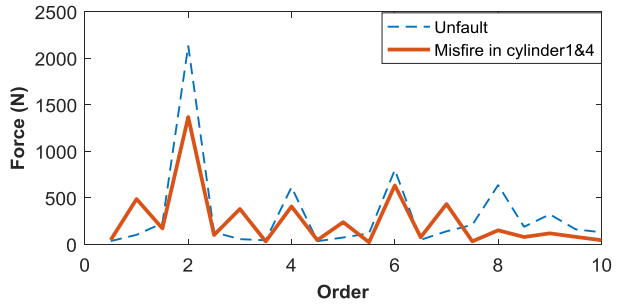

FIGURE 18. Intermittent double-cylinder misfire.

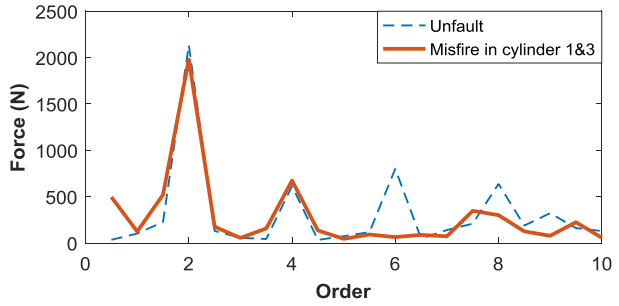

FIGURE 19. Continuous double-cylinder misfire.

and phase of the acceleration signals from the three triaxial acceleration sensors. All the misfire events are simulated at 2000 rpm. The results of the three misfire cases are shown in Figs. 17-19, respectively.

We observed that the experimental results have good consistency with the simulation results shown in Figs. 7-9. That is to say, the misfire diagnosis method based on the

identification of the generalized force at the C.G. can effectively identify different misfires.

V. CONCLUSION

In this contribution, a misfire diagnosis method based on identifying the generalized force at the C.G. is developed. The simulation results demonstrate that the method can efficiently identify different misfire faults. The fault features extracted through the simulation need to be evaluated using experimental data, so experimental vibration signals from combustion faults are studied. Meanwhile, as inputs of the simulation models, the inertia parameters of the engine and the parameters of the mounts are also measured. The experimental results yield the same fault characteristics as do those of the simulation results, which verifies the reliability of proposed method. The conclusions of the research are as follows:

Single misfire-The generalized force amplitudes of the 0.5^{th}, 1^{st}, 1.5^{th} harmonics increase sharply since the gas explosion forces of the other three firing cylinders form a new cycle, the rate of the change is half of the engine speed, and correspondingly, the 0.5^{th} harmonic and its multiples appear.

Intermittent double-cylinder misfire-The generalized force appears in the 1^{st} harmonic and its multiples due to the frequency of the gas explosion forces becoming one-half of that under normal conditions.

Continuous double-cylinder misfire- The amplitude of the 0.5^{th} harmonic increases sharply.

Further studies are to be conducted on different engines under different operating conditions to generalize these results.

REFERENCES

[1] L. Wang and J. Xiang, "A two-stage method using spline-kernelled chirplet transform and angle synchronous averaging to detect faults at variable speed," *IEEE Access*, vol. 1, pp. 22471–22485, 2019.

[2] H. Liu and J. Xiang, "A strategy using variational mode decomposition, L-kurtosis and minimum entropy deconvolution to detect mechanical faults," *IEEE Access*, vol. 1, no. 7, pp. 70564–70573, Mar. 2019.

[3] J.-W. Xiang, Z.-B. Yang, and J. L. Aguilar, "Structural health monitoring for mechanical structures using multi-sensor data," *Int. J. Distrib. Sensor Netw.*, vol. 14, no. 9, pp. 1–3, 2018. doi: 10.1177/1550147718802019.

[4] J. Xiang, Y. Lei, Y. Wang, Y. He, C. Zheng, and H. Gao, "Structural dynamical monitoring and fault diagnosis," *Shock Vibrat.*, vol. 2015, Jul. 2015, Art. no. 193831.

[5] Z. Zhi-Yong, L. Cong-Yue, C. Yin-Bo, and L. Li-Guang, "An experimental study of re-spark ignition control in misfired combustion cycle based on ion current feedback," *Transactionsof CSICE*, vol. 30, no. 1, pp. 56–61, Jan. 2012.

[6] Q. Fan, J. Bian, H. Lu, S. Tong, and L. Li, "Misfire detection and re-ignition control by ion current signal feedback during cold start in two-stage direct-injection engines," *Int. J. Engine Res.*, vol. 15, no. 7, pp. 37–47, Jun. 2014.

[7] D. N. Assanis, R. B. Poola, R. Sekar, and G. R. Cataldi, "Study of using oxygen-enriched combustion air for locomotive diesel engines," *J. Eng. Gas Turbines Power*, vol. 123, no. 1, pp. 157–166, Jan. 2001.

[8] B. Bahri, A. A. Aziz, M. Shahbakhti, and M. F. M. Said, "Understanding and detecting misfire in an HCCI engine fuelled with ethanol," *Appl. Energy*, vol. 108, pp. 24–33, Aug. 2013.

[9] A. Alkhateeb and M. Das, "A model based data normalization technique for improving performance of engine misfire detection algorithms," in *Proc. IEEE Electro/Inf. Technol. Conf.* Milwaukee, WI, USA: IEEE, Aug. 2004, pp. 115–124.

[10] R. Wei-Jun, H. Yu-Yao, and Z. Wei-Gang, "On-line diagnosis on misfire fault of internal combustion engine based on crankshaft segment acceleration," *Automot. Eng.*, vol. 32, no. 4, pp. 339–368, Apr. 2010.

[11] S. Helm, M. Kozek, and S. Jakubek, "Combustion torque estimation and misfire detection for calibration of combustion engines by parametric Kalman filtering," *IEEE Trans. Ind. Electron.*, vol. 59, no. 11, pp. 4326–4337, Nov. 2012.

[12] J. Arroyo, M. Muñoz, F. Moreno, N. Bernal, and C. Monné, "Diagnostic method based on the analysis of the vibration and acoustic emission energy for emergency diesel generators in nuclear plants," *Appl. Acoust.*, vol. 74, pp. 502–508, Apr. 2013.

[13] L. Jianmin, S. Yupeng, Z. Xiaoming, X. Shiyong, and D. Lijun, "Fuel injection system fault diagnosis based on cylinder head vibration signal," *Proc. Eng.*, vol. 16, pp. 218–223, Aug. 2011.

[14] S. Kim, H. C. Min, and S. Kooksang, "The misfire detection by the exhaust pressure ascent rate," *Trans. Korean Soc. Automot. Eng.*, vol. 11, no. 2, pp. 1–7, Mar. 2003.

[15] M. Tamura, H. Saito, Y. Murata, K. Kokubu, and S. Morimoto, "Misfire detection on internal combustion engines using exhaust gas temperature with low sampling rate," *Appl. Thermal Eng.*, vol. 31, nos. 17–18, pp. 4125–4131, 2011.

[16] P. Bogus and J. Merkisz, "Misfire detection of locomotive diesel engine by non-linear analysis," *Mech. Syst. Signal Process.*, vol. 19, no. 4, pp. 881–899, Jul. 2005.

[17] W. M. Adaileh, "Engine fault diagnosis using acoustic signals," *Appl. Mech. Mater.*, vols. 295–298, pp. 2013–2020, Feb. 2013.

[18] C. Hu, A. Li, and X. Zhao, "Multivariate statistical analysis strategy for multiple misfire detection in internal combustion engines," *Mech. Syst. Signal Process*, vol. 25, no. 2, pp. 694–703, Feb. 2011.

[19] X. Yu, L. Liu, S. Yang, X. Zhong, and D. Liu, "Misfire detection based on engine speed using wavelet," in *Proc. IEEE Intell. Vehicles Symp.* Xi'an, China: IEEE, Jun. 2009, pp. 833–837.

[20] A. W. Osburn, T. M. Kostek, and M. A. Franchek, "Residual generation and statistical pattern recognition for engine misfire diagnostics," *Mech. Syst. Signal Process.*, vol. 20, no. 8, pp. 2232–2258, Nov. 2006.

[21] S. B. Devasenapati, V. Sugumaran, and K. I. Ramachandran, "Misfire identification in a four-stroke four-cylinder petrol engine using decision tree," *Expert Syst. Appl.*, vol. 20, no. 3, pp. 2150–2160, 2010.

[22] A. Sharma, V. Sugumaran, and S. B. Devasenapati, "Misfire detection in an IC engine using vibration signal and decision tree algorithms," *Measurement*, vol. 50, pp. 370–380, Apr. 2014.

[23] C. M. Wang, *Vehicle Engine Dynamics*. Beijing, China: National Defense Industry Press, 1990, pp. 80–145.

[24] J. S. Tao, G. R. Liu, and K. Y. Lam, "Design optimization of marine engine-mount system," *J. Sound Vibrat.*, vol. 235, no. 3, pp. 477–494, Aug. 2000.

[25] C. Xu and F. Cao, "Engine excitation force identification on the basis of discrete spectrum correction," *Math. Problems Eng.*, vol. 2015, Sep. 2015, Art. no. 17525.

[26] C. Xu, K. Ding, and Z. Yang, "Identification of engine inertia parameters on the basis of frequency response functions," *Int. J. Vehicle Des.*, vol. 60, nos. 1–2, pp. 121–137, Sep. 2012.

CHUANYAN XU received the B.S. degree in computer science and technology from Liaocheng University, China, in 2005, and the Ph.D. degree from the South China University of Technology, China, in 2012. She is currently an Associate Professor with the College of Automotive Engineering, Shandong Jiaotong University, China. Her research interests include faults detection of mechanical systems and signal processing techniques.

SHAN LI received the B.S. degree in traffic specialty from Shandong Jiaotong University, China, in 2018, where she is currently pursuing the master's degree in traffic engineering. Her research interest includes faults detection of mechanical systems.

FENGPING CAO received the B.S. degree from Shandong Jiaotong University, China, in 2006, and the M.S. and Ph.D. degrees from Jilin University, China, in 2008 and 2011, respectively. She is currently an Associate Professor with the College of Automotive Engineering, Shandong Jiaotong University, China. Her research interests include the vehicle active safety and faults detection of mechanical systems.

XUYUN QIU received the B.S. and M.S. degrees from the Shandong University of Technology, China, in 2000 and 2003, respectively, and the Ph.D. degree from Tongji University, China, in 2006. He is currently a Professor with the College of Automotive Engineering, Shandong Jiaotong University, China. His research interests include faults detection of mechanical systems, and vehicle dynamics control and simulation.